CrossMark

ORIGINAL ARTICLE

Impact Fretting Wear Behavior of Alloy 690 Tubes in Dry and Deionized Water Conditions

Zhen-Bing Cai[1] · Jin-Fang Peng[1] · Hao Qian[2] · Li-Chen Tang[2] · Min-Hao Zhu[1]

Abstract The impact fretting wear has largely occurred at nuclear power device induced by the flow-induced vibration, and it will take potential hazards to the service of the equipment. However, the present study focuses on the tangential fretting wear of alloy 690 tubes. Research on impact fretting wear of alloy 690 tubes is limited and the related research is imminent. Therefore, impact fretting wear behavior of alloy 690 tubes against 304 stainless steels is investigated. Deionized water is used to simulate the flow environment of the equipment, and the dry environment is used for comparison. Varied analytical techniques are employed to characterize the wear and tribochemical behavior during impact fretting wear. Characterization results indicate that cracks occur at high impact load in both water and dry equipment; however, the water as a medium can significantly delay the cracking time. The crack propagation behavior shows a jagged shape in the water, but crack extended disorderly in dry equipment because the water changed the stress distribution and retarded the friction heat during the wear process. The SEM and XPS analysis shows that the main failure mechanisms of the tube under impact fretting are fatigue wear and friction oxidation. The effect of medium(water) on fretting wear is revealed, which plays a potential and promising role in the service of nuclear power device and other flow equipments.

Keywords Impact fretting wear · Alloy 690 · Oxidative wear · Crack · Fracture appearance

1 Introduction

As a special type of damage occurring at the contact surface, fretting can cause rapid crack formation of working components and lead to premature service failures [1]. According to the directions of the relative motions, four basic fretting modes exist, namely, tangential, radial, rotational, and torsional [2, 3]. These four models belong to the condition matched interface. Nevertheless, only a few studies focus on the separation of fretting wear modes, particularly of impact wear. Impact wear is a subtle amount of vibration that occurs on the surfaces of two objects. Numerous studies have reported that repeated impact fretting produces cracks and that the cracks propagate and cause the objects to fail. Zhao, et al [4], postulate delamination theory of wear, which is mainly concerned with deformation below the surface. Xin, et al [5], investigate that there are five layers: oxide layer, mixed layer, TTS layer, plastic deformation layer and base materials in the fretting wear subsurface. Sato, et al [6] describe the significant differences in impact-fretting wear by comparing impact-fretting wear with pure impactor with fretting, which show that dynamic corrosion followed the parabolic law of oxidation of metals and the thermal activation process.

Numerous fretting damages exist at various parts of nuclear power systems [7], such as reactor fuel assembly,

✉ Zhen-Bing Cai
  caizb@swjtu.cn

1 Traction Power State Laboratory, Southwest Jiaotong University, Chengdu 610031, China

2 Shanghai Nuclear Engineering Research and Design Institute, Shanghai 200233, China

control rod assembly [8], reactor component, steam generator, pressure vessel [9], main pump, and coolant pump. The steam generator is a key equipment in nuclear power systems, and fretting damage is one of the main reasons [10] causing its failure. With high thermal strength, good corrosion resistance, anti-oxidation, and other characteristics, alloy 690 is extensively used in the nuclear power and aerospace fields. In nuclear power plants, U-tubes in the steam generator are supported by structures called egg crates. Flow-induced vibration of the U-tubes causes wear to occur on the zone of contact and generates combinations of impacting and sliding motions between the U-tube against the support [11–14]. Recently, most of the domestic and foreign studies on wear have concentrated on the sliding wear or bending behavior of the steam generator tubes. In another study, bending (four-point or three-point bending) has been used to determine the damage behavior of tubes or rods [15]. Gueout, et al [16] report that wear of pure sliding is larger than impact wear in the case of anti-vibration bar testing. In particular, the wear amount of impact sliding increase more than that of pure sliding or impact wear test. Jeong, et al [17], indicate that the friction coefficient in air is higher than that in water. The friction coefficient and wear rate increased as the temperature of water increase in the water environment. Chung, et al [18], conclude that the wear coefficient in ambient room temperature is lower than 80 °C in water conditions and explain that the protective nature of the tribologically transformed layers could decrease the wear volume. Most of study focus on the tangential fretting wear of alloy 690

tubes, and research on impact fretting wear of alloy 690 tubes is limited. The impact fretting wear behavior of alloy 690 is significant in the evaluation of the life of steam generator tubes in nuclear power plants and in better understanding the wear mechanisms of steam generator tube materials.

In this study, an impact fretting wear simulator was demonstrated to elucidate the impact wear behavior under the dry and deionized water conditions at room temperature.

2 Experimental Method and Materials

2.1 Specimen Preparation

The test materials used in this study were alloy 690 and commercial nickel-based alloys as steam generator tube materials in nuclear power plants. The dimensions of the tube specimens were 17.48 mm diameter, 1 mm wall thickness, and 10−15 mm length. The counterpart materials were 405 stainless steel used as tube support materials (anti-vibration bar) in the power plants, which were cut into plate specimens with 8 mm × 8 mm × 25 mm size. These plates were ground with sandpaper until their roughness reached $Ra = 0.02$ μm. The chemical compositions of the two tested materials are shown in Table 1. Prior to the test, tall tribo-pair specimens were cleaned with acetone by ultrasonic cleaning instrument.

Table 1 Chemical composition of wear tested materials (wt%)

Specimen	C	Si	Mn	Ni	Cr	Fe
690 alloy	0.015–0.025	≤0.50	≤0.50	≥58	28.5–31	9.0–11.0
405 SS	0.07	0.87	1.08	–	13.80	Balance

*Cycle below 10^6, cracks appeared at the contact zone in the tubes

Fig. 1 Schematic of the impact in the nuclear power device and its impact fretting wear tester. 1. Vibration exciter; 2. Force and acceleration transducer; 3. Upper clamp; 4. Plate specimen; 5. Tube specimen; 6. Lower fixer; 7. Container

(a) Nuclear power plant   **(b)** Impact wear rig
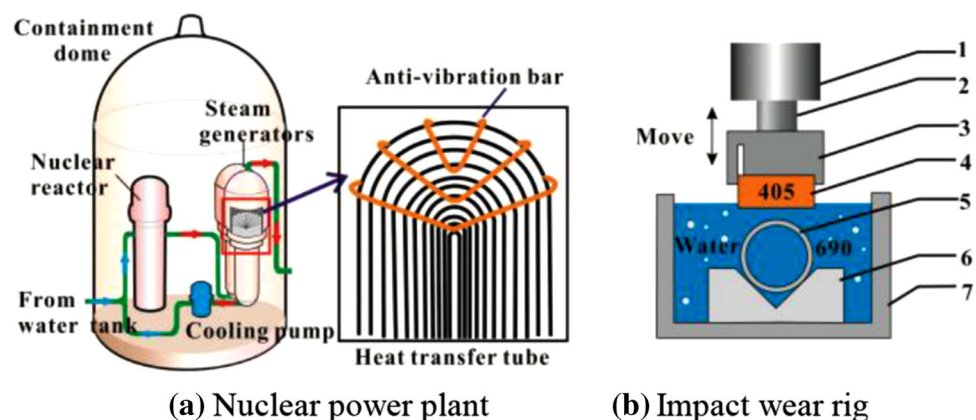
2.2 Impact Fretting Test

A small displacement impact wear testing machine with tube-on-plate configuration had been developed to simulate the impact fretting wear phenomenon between the tube and the support material, as shown in Fig. 1.

As shown in Fig. 1, alloy 690 tube was fixed in a "V" groove fixture, the load sensor was connected to the vibrator, and the plate specimens were installed under the load sensor by the upper fixture. During the test, the impact wear test used a force control mode. The impact force could be changed by adjusting the magnitude of the

Table 2 Number of impact cycles in different loads and tube ($\times 10^5$)

Tube length L/mm	Lubrication condition	Impact load F_n/N				
		20	30	40	45	50
10	Dry	10	10	3	2.2	1.3
10	Water	10	10	10	3.9	1.8
15	Dry	10	10	10	10	9
15	Water	10	10	10	10	10

Fig. 2 Morphologies and 2D profiles of the wear scars in the dry water condition, $L = 15$ mm
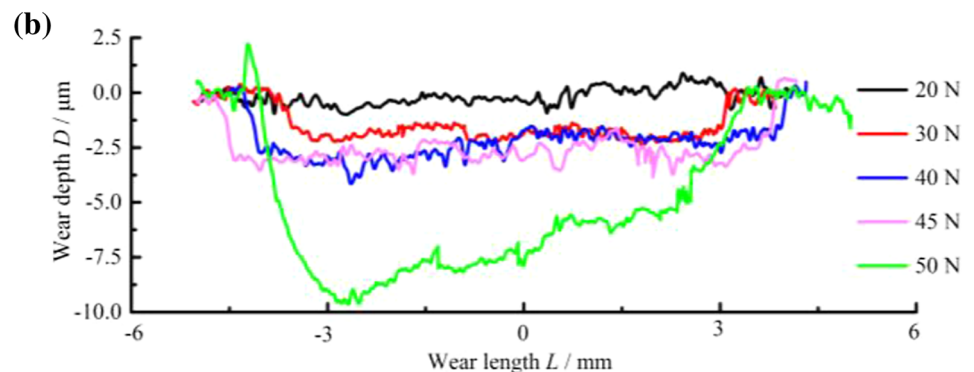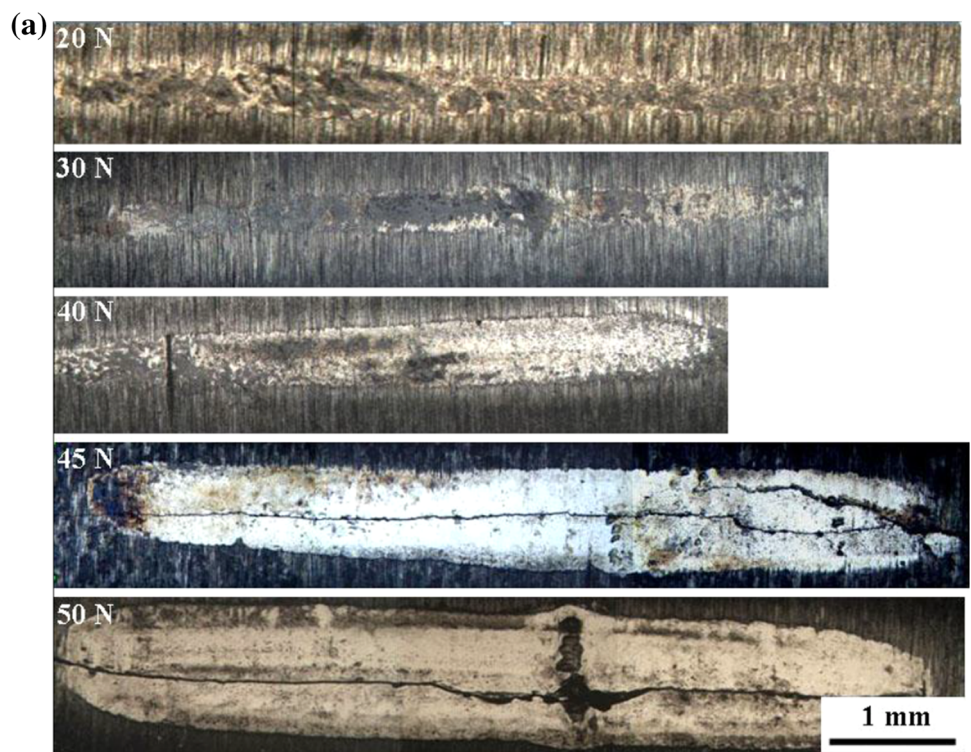
Fig. 3 Morphologies and 2D profiles of the wear scars in the deionized water condition, $L = 15$ mm
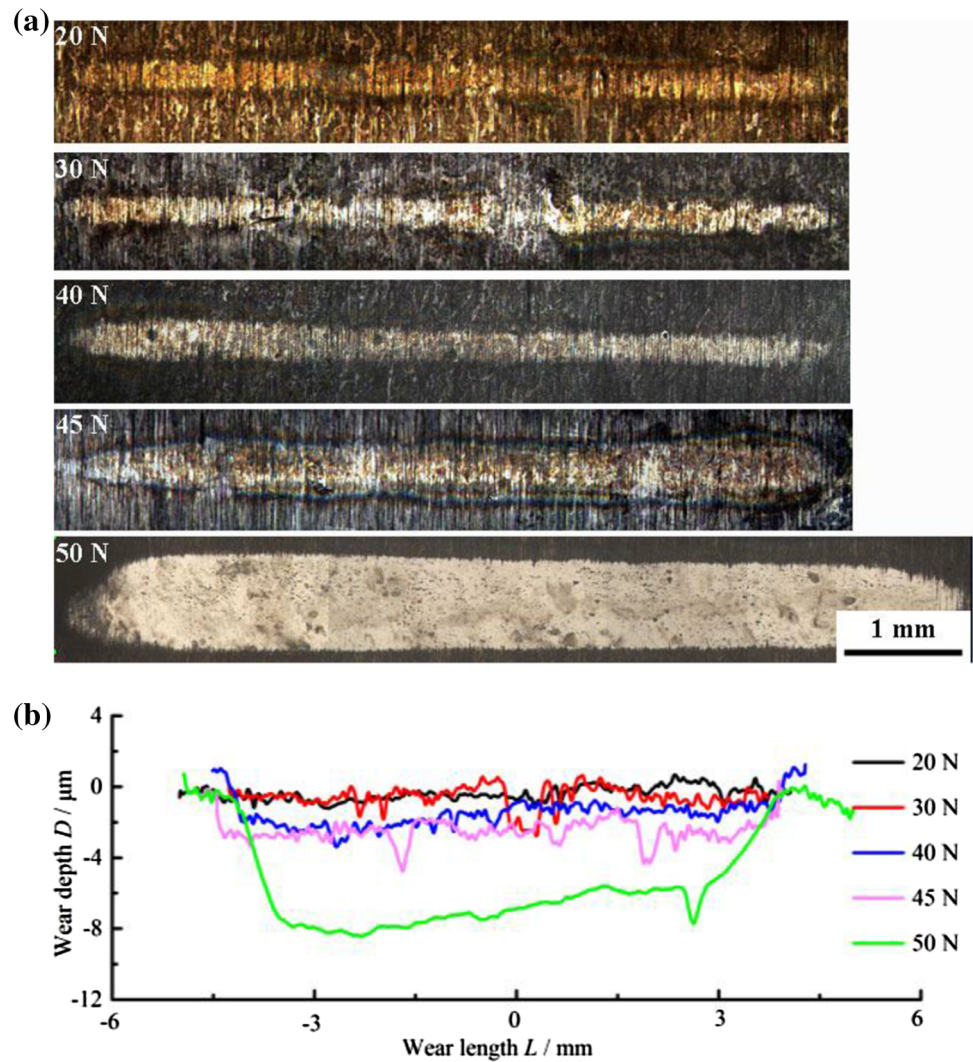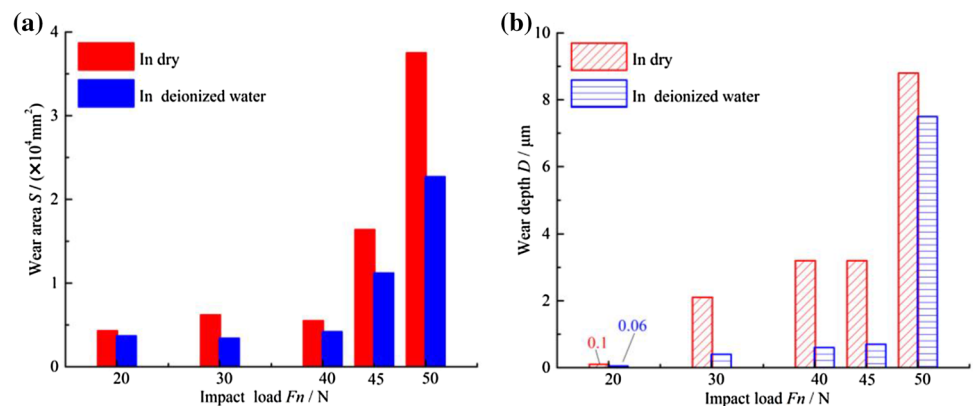

Fig. 4 Wear area and depth of wear surface under different loads, $L = 15$ mm

current. When the tube was impacted by the plate, the impact contact force can be measured by the load sensor. The impact block was raised when the peak force was reached. Two types of lubrication conditions, namely, dry and water(deionized water), were obtained at room temperature. A frequency of 5 Hz of the 1 mm impact distance and 10^6 cycles were selected in all the tests, and the applied normal peak loads were set as 20 N, 30 N, 40 N, 45 N, and 50 N. A visual monitoring device observed the status of the interface during the test. If a macroscopic crack was observed on the tube surface, then the test was stopped and the computer recorded the cycle number.
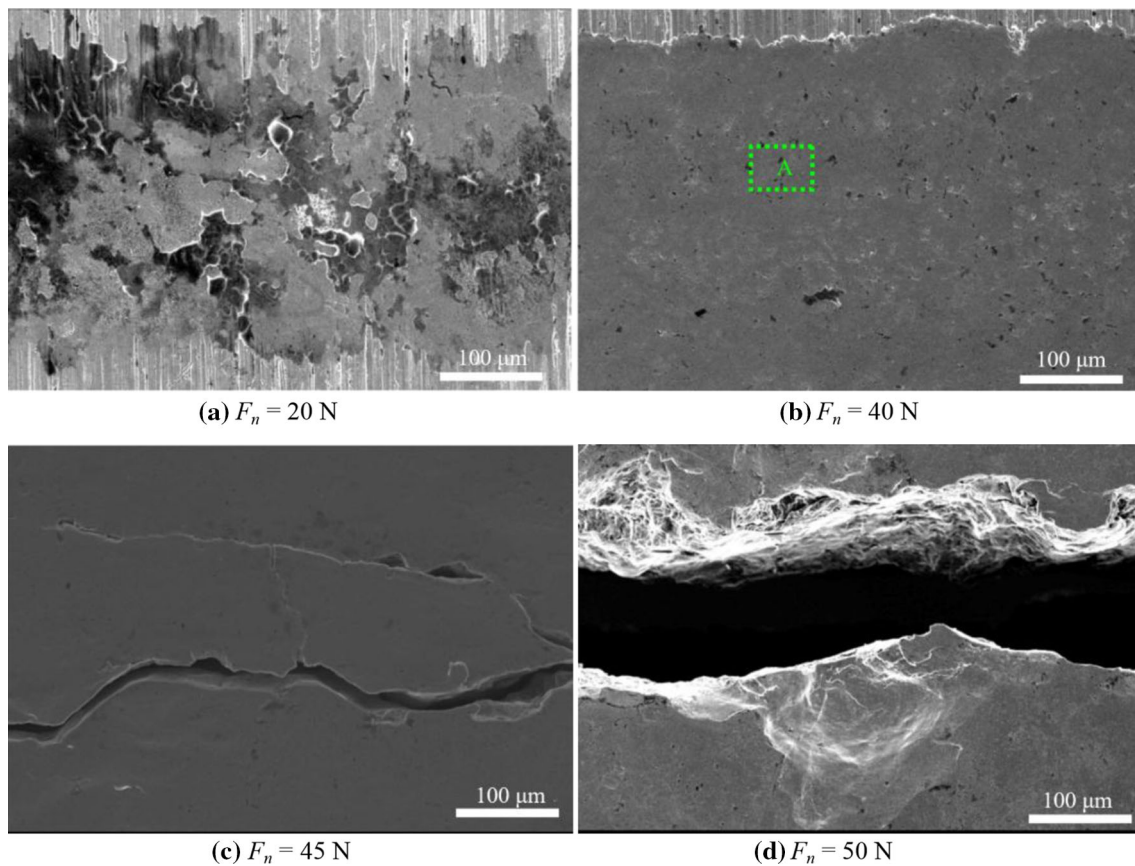
(a) $F_n = 20$ N

(b) $F_n = 40$ N

(c) $F_n = 45$ N

(d) $F_n = 50$ N

Fig. 5 SEM microphotograph of the worn surface in the dry water condition, $L = 15$ mm

2.3 Analysis Methods

After the wear test, the wear scar was observed by using the white light interferometer(Contour GT type) and the wear area was calculated. Various surface imaging and chemical analysis techniques were conducted to reveal the wear and damage mechanisms. These techniques included optical microscopy (OM, OLYMPUS BX50 Japan), scanning electron microscopy (SEM, JEOLJSM-6610LV), energy-dispersive X-ray spectroscopy(EDX, OXFORD X-MAX50 INCA-250), and X-ray photoelectron spectroscopy(XPS, Thermofisher Scientific, ESCALAB 250Xi).

3 Results and Discussion

3.1 Wear Behavior

The impact number under different loads in the dry and deionized water conditions is shown in Table 2. Several characteristics are observed as follows.

(1) With the increase in the applied normal load, the time or fracture is shorter.

(2) The 10 mm long tubes easily crack in the same condition. For example, after increasing the length of the tube, the number of fracture increases from 3×10^5 cycles to 9×10^5 cycles because long tubes have better flexibility and can absorb more energy from wear and impact processing.

(3) Compared with the impact of tube in dry and deionized water, when the tube cracks in dry water, the deionized water lubrication can significantly delay the cracking time. The cycle of crack appearance increases from 1.3×10^5 to 1.8×10^5 when the impact load set as 50 N. Figure 2 shows the OM and 2D profiles of the wear scar of the 15 mm long tube in dry water. Increasing the impact loads results in serious wear of the morphology of the tube. Particularly when the load increases to 45 N, the tube cracks until the end of the test. Wear depth increases from 1 μm to 10 μm when the impact load increase from 20 N to 50 N. The uplift phenomenon is observed at the edge of the wear surface. This phenomenon indicates that the extrusion deformation of material occurs during impact fretting wear and remains negligible in smaller load.
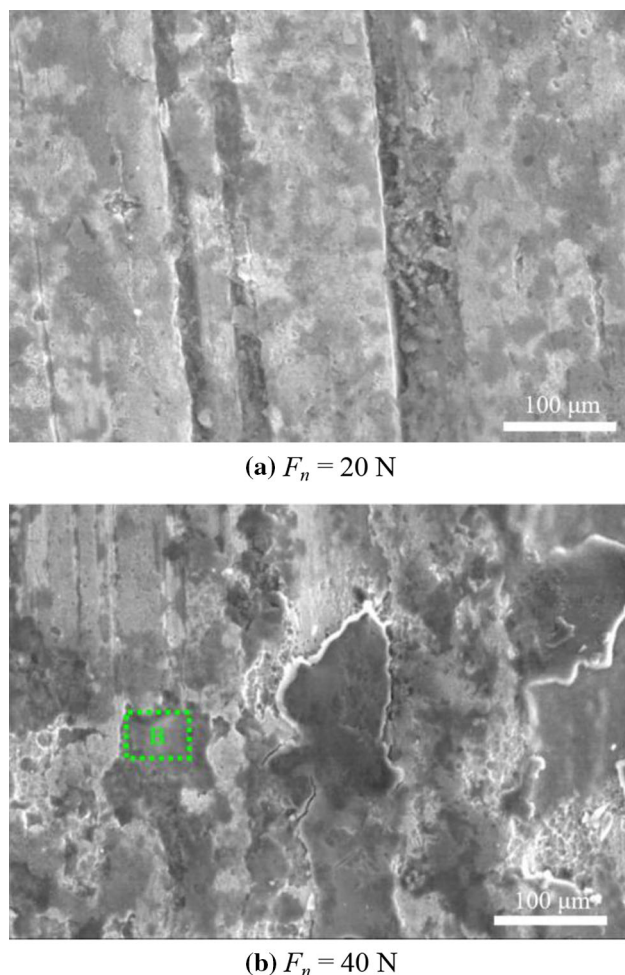
(a) $F_n = 20$ N

(b) $F_n = 40$ N

Fig. 6 SEM microphotograph of the worn surface in the deionized water condition, $L = 15$ mm
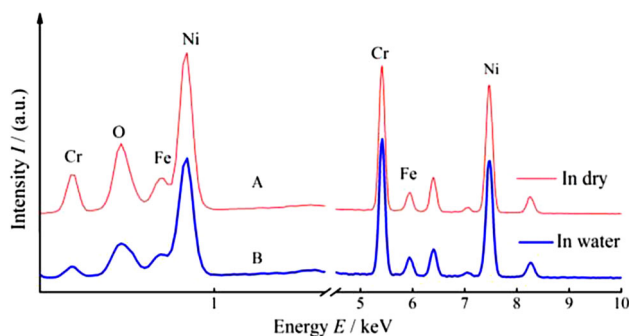

Fig. 7 EDX spectrum of the worn surface (corresponding to the green zone in Figs. 5(b) and 6(b))

The OM and 2D profiles of the wear scar of the 15 mm long tube in deionized water are shown in Fig. 3. Between the OM and 2D profiles of the impact wear scar in the dry and deionized water conditions, the impact wear depth is smaller in the deionized water condition than that in the dry

water condition. The maximum wear depth was approximately 8 μm in water.

Figure 4 shows the wear area and depth in the two types of lubrication conditions. Generally, the wear area is linearly dependent on the applied load and the lubrication induces the reduction in wear. However, Fig. 4 also shows that the wear depth and area do not increase linearly with the increase in load. When the impact load is lower than 40 N, the values of the wear area and depth slightly change. When the load increases to 50 N, the wear area was 1.8 times that of the value in dry water because if the contact stress is higher than a certain level, then severe plastic deformation accompanied by abrasive wear lead to considerable material loss [19]. In the dry water condition, the debris from the loose material could form a three-body bed, separate the contact interface, and reduce wear. However, in this test, the contact zone has a curved surface and the loose material is easily removed. Thus, a dark worn surface is not observed in Fig. 2. The wear area and depth in deionized water were less than that in dry water, which was understandable. Wang [20] propose that the damping effect decrease the wear rates in the deionized water during the same motivation support conditions.

Figure 5 shows the microphotograph of the worn surface in the dry water condition. When the impact load was set as 20 N, worn particles are observed on the plastically deformed surface. When the load set as 40 N, the wear becomes serious. Particles are rarely observed on the worn surface because the surface is pressed, compact, and tidy. Cracks appear at 45 N; two intersecting cracks are visible at the edge of the wear scar (Fig. 5c), and a crack runs through the entire tube at 50 N. Damage accumulation cause the material to be unable to resist the continuous impact stress. Figure 6 shows the wear microphotograph of the worn surface in the deionized water condition. When the impact load set as 20 N, wear is slight and the surface of the original machining marks is observed (Fig. 6a). A small amount of delamination layer is observed on the worn surface. On one hand, water has a lubricating effect that modifies the contact surface stress and friction during the test. On the other hand, the liquid was conducive to the spread of friction heat.

The worn surface compositions were investigated by using EDX (Fig. 7) in the dry and deionized water conditions. The "A" and "B" positions are selected for EDX in the scar, as shown in Figs. 5 and 6. The EDX results indicated that oxidative wear was one of the crucial damage effects for the tube sample under the impact wear condition. Compared with the dry water condition, the oxygen content of the worn sample in the deionized water condition is lower. Thus, the impact wear loss in the dry water condition is more serious than that in the deionized water condition.
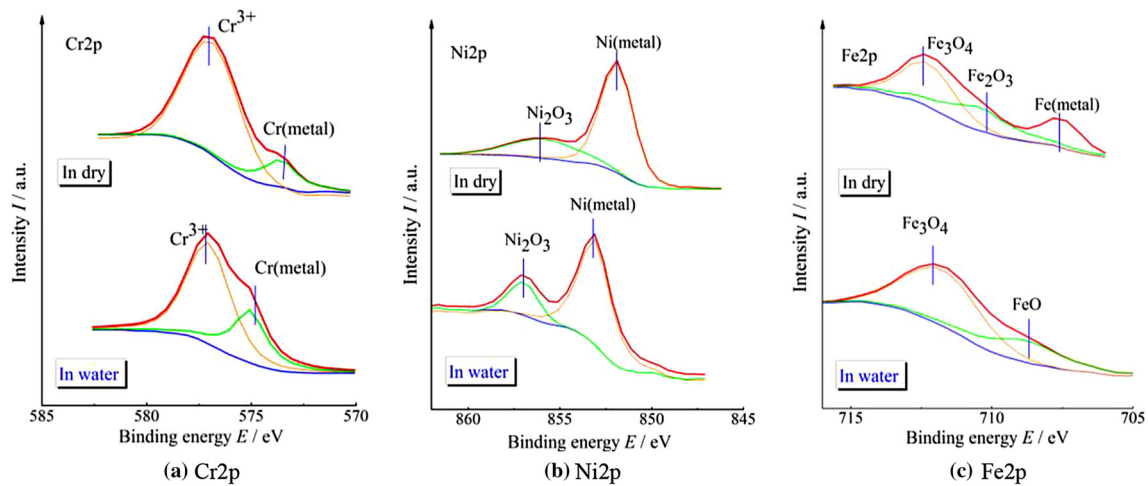
Fig. 8 XPS spectra of the wear scars in the dry and deionized water conditions: $F_n = 40$ N, $L = 15$ mm

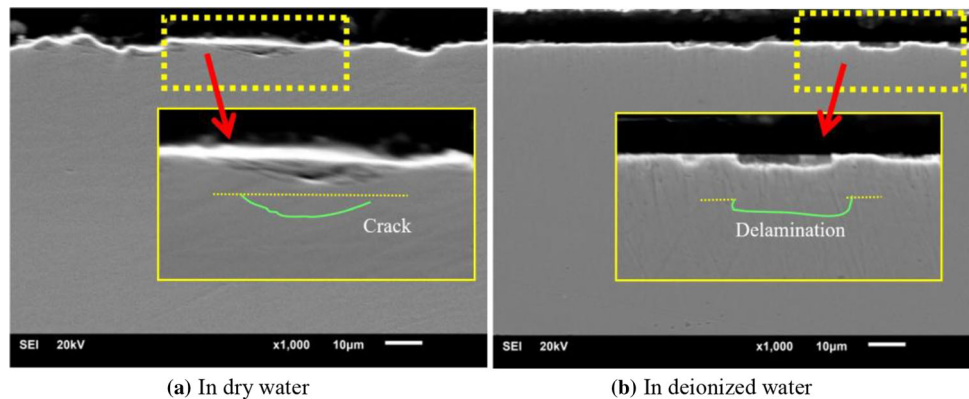**Fig. 9** SEM micrographs of the cross-section of the wear scar, $F_n = 50$ N, $L = 15$ mm

(a) In dry water

(b) In deionized water

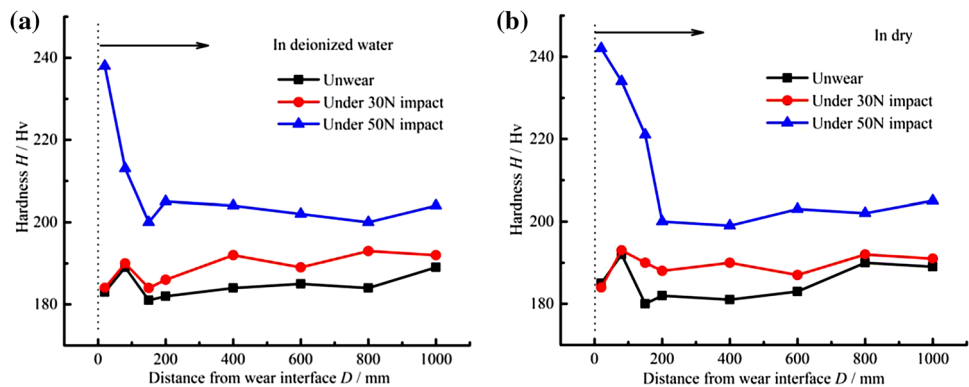**Fig. 10** Hardness of the cross-section from worn surface to inner layer, $L = 15$ mm

Figure 8 shows the XPS spectra of Cr2p, Ni2p, and Fe2p from the scar surfaces in the dry and deionized water conditions. As shown in Fig. 8a, two typical peaks in the spectrum of Cr2p$_{3/2}$ are observed. The peak observed at 577.3 eV is ascribed to Cr_2O_3, and the other peak is ascribed to Cr (its binding energy is 574.3 eV), Cr(III) oxide fit with multiplet as shown above and fit Cr metal with asymmetric peak, Native oxide on Cr metal may be a mix of Cr(III) oxide and Cr(III) hydroxide [21]. From

Ni2p$_{3/2}$ of the spectrum shown in Fig. 8b, two peaks are observed: one peak is Ni_2O_3 (its binding energy was 856.3 eV) and the other peak is Ni (its binding energy is 852.5 eV) [22]. Three peaks are observed in the XPS spectra of Fe2p in the dry water condition (Fig. 8c). The binding energy of Fe_3O_4 is 712.4 eV, the binding energy of Fe_2O_3 is 710.6 eV, and the binding energy of Fe is 706.8 eV. Two peaks are observed in the XPS spectra of Fe2p from the scar surface in the deionized water
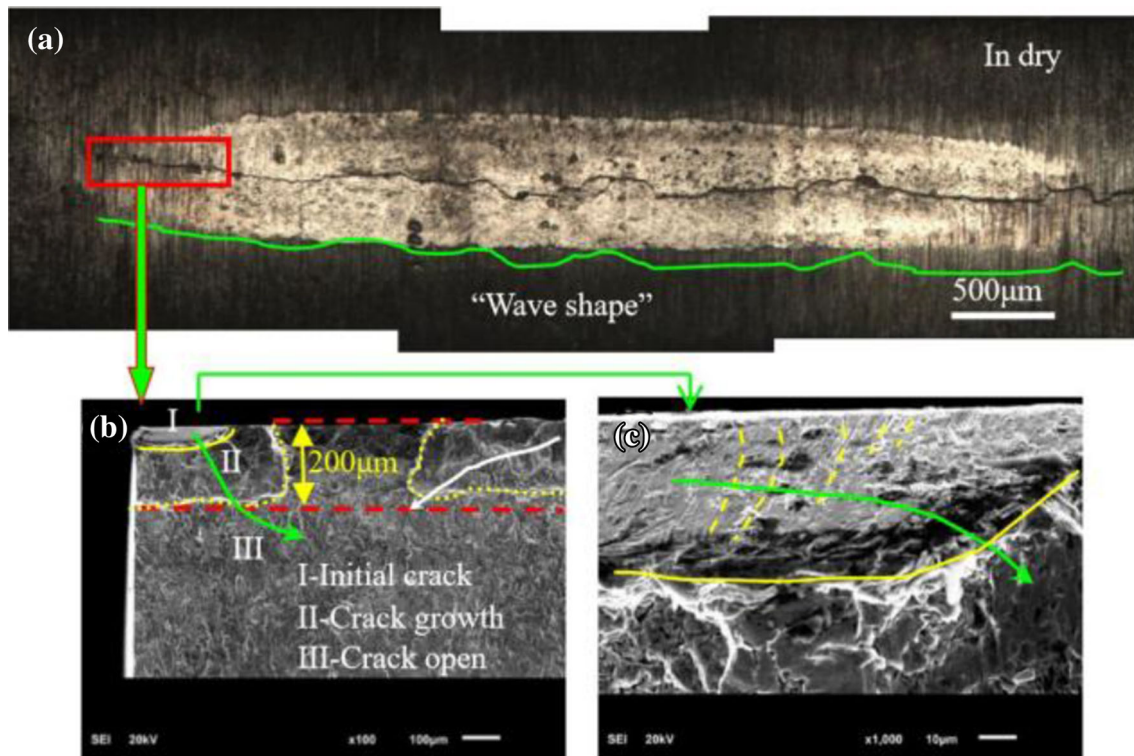
Fig. 11 Morphology of impact crack and fracture appearance in the dry water condition, $F_n = 50$ N, $L = 10$ mm

condition: one peak is Fe_3O_4 (its binding energy is 712.4 eV) and the other peak is FeO (its binding energy is 709.5 eV) [23]. The XPS results of the elements Cr and Ni show that the chemical compositions of the worn surfaces of the dry and deionized water conditions are similar. The Cr_2O_3 and Ni_2O_3 peaks are observed in the two types of lubrication conditions. The results of the element Fe show that the chemical compositions of the scar surfaces of the dry and deionized water had several differences. The Fe_2O_3 and Fe_3O_4 peaks are observed in the scar surface of the dry water condition. The FeO and Fe_3O_4 peaks appears in the scar surface of the deionized water condition.

3.2 Fatigue Behavior

Figure 9 illustrates the SEM micrographs of the cross-section of the wear scar in the two types of lubrication conditions. A micro-crack with 20 μm length parallel to the surface is observed in the dry water condition (Fig. 9a). The crack does not appear in the deionized water condition. In Fig. 9b, only the delamination layer can be observed, indicating that the impact of fretting wear causes fatigue wear of the surface material and that the expansion of the fatigue crack leads to spall. These subsurface small cracks induce the formation of cracks in the tube.

The micro hardness tests were conducted along the depth direction from the worn surface. On each tube

specimen, the hardness tests are conducted at different locations and the average values are plotted in Fig. 10. Prior to the impact wear test, the hardness value of the tube is 190 HV. However, the hardness near the worn surface rapidly increases with the increase in the impact load regardless of the water or dry state. Within 1 mm of the subsurface, the impact load has a remarkable effect on hardness and a high load lead to higher secondary surface hardness.

Fracture appearance is investigated, including fracture appearance in the dry and deionized water conditions, to determine the mechanism of the fracture of the tube under the impact condition. In particular, when the length of the tube is 10 mm and the impact load set as 50 N, the fracture of the tube is evident. Figure 11 and Fig. 12 show that the morphology of the crack in the dry water condition is different from the morphology of the crack in the deionized water condition. Figure 11 shows the fracture appearance in the dry water condition. Fracture appearance is a typical fatigue characteristic [24], and many crack sources are observed because of the form of the line contact applied during the impact test. In the subsurface layer, several slip lines can be observed because of dislocation slips under the impact load (Fig. 11c). In this result, the deformed layer is observed from surface to the depth of $150 - 200$ μm. In the study of Yang [25], cracks easily form in the deformation layer. Figure 12 shows the fracture appearance in
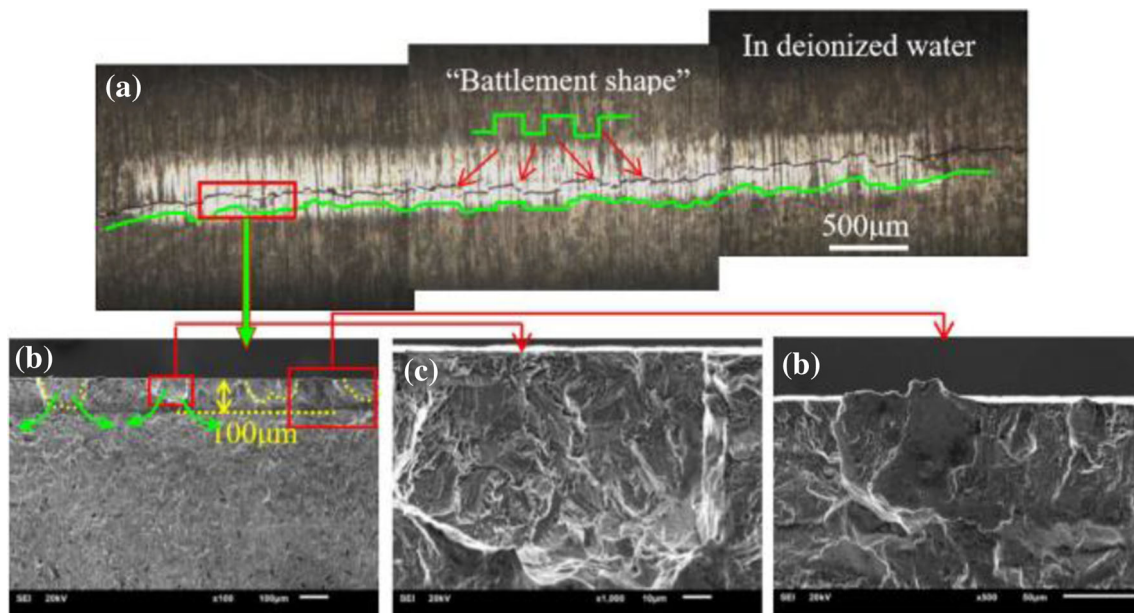
Fig. 12 Morphology of crack and fracture appearance in the deionized water condition, $F_n = 50$ N, $L = 10$ mm

the deionized water condition. The quasi-cleavage characteristics are observed, and the contact stress is small because of the presence of the deionized water film. The material shows a formation of a deformation layer, and the impact wear is small under the impact test. The material is separated along a certain crystallographic plane. In the deionized water condition, the wear scar was slight. The traces of the original processing can also be observed. The crack propagation morphology shows a jagged shape (similar to the battlement shape) in the water, but extends disorderly in the dry condition. The results of Meng's study [26] shows that stress corrosion cause the tube to crack in the fluid condition, and the cracks extend along the grain boundaries. Thus, the crack of the wear surface exhibits a "wave shape" in the deionized water condition. This phenomenon does not occur in the dry water condition. In the analysis of crack fractures in tubes, a quasi-cleavage fracture characterized by river pattern and cleavage terrace is observed and confirmed.

4 Conclusions

(1) The impact wear gradually increased with the increases in impact load from 20 N to 50 N. Oxidative wear and delamination are the dominant mechanisms of wear. The oxidative wear decrease apparently because of the protection of the fluid.

(2) Cracking occurs at high loading and the tube with a short length. However, the deionized water lubrication can significantly delay the cracking time.

(3) The main failure mechanism during impact fretting wear is fatigue wear in water and oxidation wear in the dry condition. The crack of the wear surface is different in the dry and deionized water condition. Stress corrosion has an effect on the cracking behavior in water.

References

1. A Ramalho, A Mertallinger, A Cavaleiro. Fretting behaviors of W-Si coated steels in vacuum environment. *Wear*, 2006, 261(1): 79–85.
2. Z B Cai, M H Zhu, Z R Zhou. An experimental study of torsional fretting behavior of LZ50 steel. *Tribology International*, 2010, 43(1): 361–369.
3. Z B Cai, G Zhang, Y Zhu, et al. Torsional fretting wear of nitrogen ion implantation biomedical Ti6Al7Nb alloy under bovine serum. *Tribology International*, 2013, 59: 312–320.
4. L Zhao, J Hu, Z Wu, et al. Investigation on flow accelerated corrosion mitigation for secondary circuit piping of the third Qinshan nuclear power plant. *Chinese Journal of Mechanical Engineering*, 2011, 24(2): 214–219.
5. L Xin, B Yang, Z Wang, et al. Microstructural evolution of subsurface on Inconel 690TT alloy subjected to fretting wear at elevated temperature. *Materials & Design*, 2016, 104: 152–161.

6. Y Sato, A Iwabuchi, M Uchidate, et al. Dynamic corrosion properties of impact–fretting wear in high − temperature pure water. *Wear*, 2015, 330: 182–192.

7. H Tang. Fretting damage one of worldwide difficulties in the field of nuclear power equipment and structures for a long term. *Nuclear Power Engineering*, 2000, 21(3): 222–231.

8. L Yang, M Zhou, Z Tian. Heat transfer enhancement with mixing vane spacers using the field synergy principle. *Chinese Journal of Mechanical Engineering*, 2016, 30(1): 127-134.

9. Y Zhong, C Zhou, S Chen, et al. Effects of temperature and pressure on stress corrosion cracking behavior of 310S stainless steel in chloride solution. *Chinese Journal of Mechanical Engineering*, 2016, 30(1): 200-206.

10. H Jiang, J Qu, R Y Lu, et al. Grid-to-rod flow-induced impact study for PWR fuel in reactor. *Progress in Nuclear Energy*, 2016, 91: 355–361.

11. K Fujta. Flow − induced vibration and fluid − structure interaction in nuclear power plant components. *Journal of Wind Engineering and Industrial Aerodynamics*, 1990, 33(1-2): 405–418.

12. J Luo, Z B Cai, J L Mo, et al. Friction and wear properties of high-velocity oxygen fuel sprayed WC-17Co coating under rotational fretting conditions. *Chinese Journal of Mechanical Engineering*, 2016, 29(3): 515–521.

13. H G D Goyder. Flow − induced vibration in heat exchangers. *Chemical Engineering Research and Design*, 2002, 80(3): 226–232.

14. P Ko, A Lina, A Ambard. A review of wear scar patterns of nuclear power plant components. *ASME 2003 Pressure Vessels and Piping Conference*, USA, 2003: 97–106.

15. L Guo, S Yang, H Jiao. Behavior of thin-walled circular hollow section tubes subjected to bending. *Thin-Walled Structures,* 2013, 73: 281–289.

16. F M Gueout, N Fisher. Steam generator fretting − wear damage: A summary of recent findings. *Journal of Pressure Vessel Technology*, 1999, 121(3): 304–310.

17. S Jeong, C Cho, Y Lee. Friction and wear of Inconel 690 for steam generator tube in elevated temperature water under fretting condition. *Tribology International*, 2005, 38(3): 283–288.

18. I Chung, M Lee. An experimental study on fretting wear behavior of cross − contacting Inconel 690 tubes. *Nuclear Engineering and Design*, 2011, 241(10): 4103 − 4110.

19. J Li, Y Lu, H Zhang, et al. Effect of grain size and hardness on fretting wear behavior of Inconel 600 alloys. *Tribology International*, 2015, 81: 215–222.

20. T Wang, S Shen. Experimental studies of fretting wear in heat exchanger tubes. *Nuclear Power Engineering*, 1990, 11(6): 338–443.

21. B Payne, M Biesinger, N Mcintyre. X-ray photoelectron spectroscopy studies of reactions on chromium metal and chromium oxide surfaces. *Journal of Electron Spectroscopy and Related Phenomena*, 2011, 184(1): 29 − 37.

22. A Grosvenor, M Biesinger, R Smart, et al. New interpretations of XPS spectra of nickel metal and oxides. *Surface Science,* 2006, 600(9): 1771 − 1779.

23. Y Toru, H Petr. Analysis of XPS spectra of Fe^{2+} and Fe^{3+} ions in oxide materials. *Applied Surface Science*, 2008, 254(8): 2441 − 2449.

24. Q P Zhong, Z H Zhao. Fractography. Beijing: *Higher Education Press,* 2006.

25. W Kilian, P W Magdalena, G Sergo, et al. Sequence of deformation and cracking behaviours of Gallium-Arsenide during nano-scratching. *Materials Chemistry and Physics*, 2013, 138(1): 38–48.

26. F Meng, J Wang. Scratch-induced stress corrosion cracking for steam generator tubings. *Corrosion & Protection*, 2013, 12(5): 2114 − 2125.

Zhen-Bing Cai, born in 1981, is currently a professor at *School of Mechanical Engineering, Southwest Jiaotong University, China.* He received his bachelor PhD degree from Southwest Jiaotong University, China, in 2009. His research interests include friction and wear, surface engineering. E−mail: czb−jiaoda@126.com

Jin-Fang Peng, born in 1984, is currently an assistant research fellow in *Traction power state laboratory, Southwest Jiaotong University, China.* He received his bachelor PhD degree from Southwest Jiaotong University, China, in 2012. His research interests include friction and wear, surface engineering. E−mail: jinfangpeng3256@163.com

Hao Qian, born in 1982, is currently a senior engineer at *Shanghai Nuclear Engineering Research and Design Institute,China.* He received his master degree in 2007 from Shanghai University, China. His research interests include mechanics and nuclear safety. E−mail: qianhao@snerdi.com.cn

Li-Chen Tang, born in 1985, is currently a senior engineer at *Shanghai Nuclear Engineering Research and Design Institute,China.* He received his bachelor PhD degree from Fudan University, China, in 2013.His research interests include mechanics and nuclear safety. E−mail: tanglichen@snerdi.com.cn

Min-Hao Zhu, born in 1968, is currently a professor at *School of Mechanical Engineering, Southwest Jiaotong University, China.* He received his bachelor PhD degree from Southwest Jiaotong University, China, in 2001. His research interests include friction and wear, surface engineering and materials science. E−mail: zhuminhao@swjtu.cn